Available online at www.sciencedirect.com
ScienceDirect
Spectrochimica Acta Part A 68 (2007) 669–679
SPECTROCHIMICA ACTA PART A
www.elsevier.com/locate/saa

Vibrational spectroscopy of resveratrol

Ferenc Billes [a,*], Ildikó Mohammed-Ziegler [b], Hans Mikosch [c], Ernő Tyihák [d]

[a] *Department of Physical Chemistry, Budapest University of Technology and Economics, H-1521 Budapest, Budafoki út 8, Hungary*
[b] *H-2521 Csolnok, Arany J. u. 28, Hungary*
[c] *Institute for Chemical Technologies and Analysis, Vienna University of Technology, A-1060 Wien, Getreidemarkt 9, Austria*
[d] *Plant Protection Institute, Hungarian Academy of Sciences, H-1022 Herman Ottó út 15, Hungary*

Received 6 October 2006; received in revised form 20 December 2006; accepted 20 December 2006

Abstract

In this article the authors deal with the experimental and theoretical interpretation of the vibrational spectra of *trans*-resveratrol (3,5,4′-trihydroxy-*trans*-stilbene) of diverse beneficial biological activity. Infrared and Raman spectra of the compound were recorded; density functional calculations were carried out resulting in the optimized geometry and several properties of the molecule. Based on the calculated force constants, a normal coordinate analysis yielded the character of the vibrational modes and the assignment of the measured spectral bands.

Keywords: Resveratrol; Vibrational spectra; Atomic net charges; Stilbenoid; Quantum chemistry; Normal coordinate analysis

1. Introduction

Resveratrol (3,4′,5-trihydroxy-*trans*-stilbene) is a common phytoalexin (plant antibiotic) which can be found in at least 72 species of plants distributed among 31 genera and 12 families [1,2]. All of the plant families which are found to contain resveratrol belong to the spermatophytes division as e.g., Vitaceae, Myrtaceae [3,4]. It is especially interesting that resveratrol has often been reported in edible and nonedible plants, alike. Foods known to contain resveratrol are limited to grapes (mainly in skins), wine, peanuts, cranberries etc. [5–7]. According to recent observations resveratrol and its glucosides as *trans*- and *cis*-piceid are present in hop, cocao and chocolate, as well [8,9].

The epidemiologic finding of an inverse relationship between consumption of red wine and incidence of cardiovascular disease has been called the "French paradox" [10]. After this finding extensive research during the last two decades has led to the conclusion that besides cardioprotective [10] and antimicrobial effects (e.g. [3]), resveratrol also exhibits anticancer properties, as suggested by its ability to suppress proliferation of a wide variety of tumor cells [1,2]. The up-to-date beneficial effects of resveratrol, in general, can be divided into two main groups: protective/chemopreventive (e.g. resveratrol increases the concentration of the high-density lipoprotein cholesterol in blood [11]) and inhibiting/killing effects [12]. Among the beneficial effects of resveratrol, its killing–inhibiting activities make it especially attractive. It acts as a pleiotropic biological effector to regulate the three major stages of chemical carcinogenesis as initiation, promotion and progression that underlie malignant transformation [1,2]. More recently, it has been observed that resveratrol induces apoptosis [2,13] and selectively inhibits leukemia cells [14].

It follows from these results that resveratrol as a common dietary agent has a special distinguished place among the dietary compounds and the common grape berries are one of the most important medicinal plants [12]. The biosynthesis of the resveratrol compound from malonic acid is very complicated. The biocatalyst is Coenzyme A in three partial processes [15].

Resveratrol was already studied with some theoretical and several experimental spectroscopic methods. Nero et al. [16] applied the semiempirical PM3/CI method for the quantum chemical calculations of the molecular geometry of resveratrol and some similar molecules and studying the possible configurations. They used the INDO/S-CI program for the computation of the UV–VIS, fluorescence and phosphorescense spectra of the molecules. They extended their calculations later [17] with RHF/6–31G* ab initio calculations for the geometry optimization of resveratrol.

* Corresponding author. Tel.: +36 1 463 1267; fax: +36 1 463 3767.
E-mail addresses: fbilles@mail.bme.hu (F. Billes), mohazihu@yahoo.com (I. Mohammed-Ziegler), hans.mikosch@tuwien.ac.at (H. Mikosch), etyih@nki.hu (E. Tyihák).

1386-1425/$ – see front matter © 2007 Elsevier B.V. All rights reserved.
doi:10.1016/j.saa.2006.12.045

Cao et al. [18] dealt with radicals, originated from resveratrol. Using the DFT B3LYP/6–31G* method they investigated the activities of the –C–O• type radicals of resveratrol. Ab initio DFT geometry optimization on the isolated resveratrol molecule were carried out by Caruso et al. [19], too.

Edelmann et al. measured its infrared spectrum [20], Scanlan et al. dealt with its resonance Raman spectrum [21]. Lin and Chen recorded the low-temperature fluorescence spectrum of the compound [22]. The mass spectrum of resveratrol was published – among others – by Dominguez et al. [23].

2. Experimental

The observed resveratrol was a Sigma–Aldrich product (99% of purity) and was applied without any purification.

The infrared spectrum of the compound was recorded in KBr pellet, on a Nicolet Magna 750 FT-IR spectrometer in the 4000–400 cm^{-1} region. Five hundred and twelve scans were accumulated. The resolution was 1 cm^{-1}.

The Raman spectrum was measured in solid state with a Nicolet FT-Raman Model 950 spectrometer equipped with an Nd:YAG laser emitting at its 1064 nm line. Five hundred and twelve scans were accumulated at a resolution of 2 cm^{-1}. For comparing the effect of the wavelength of excitation, three other Raman spectra were recorded on a Jobin-Yvon LabRam 300 dispersive micro Raman system equipped with a multichannel CCD detector using the 950 grooves mm^{-1} grating. The Raman microscope operated with a diode laser at 785 nm, a helium–neon laser at 633 nm, and a frequency-doubled Nd:YAG laser at 532 nm. In these cases, the spectral resolution varied with the wavelength but was typically under 3 cm^{-1}. The Raman spectra were measured in the 4000–150 cm^{-1} region.

3. Computational details

Quantum chemical calculations were applied for the support of the experimental assignment of the resveratrol spectra. The Gaussian 03 program package [24] was used with the Becke3P86 hybrid functional (density functional theory) and the 6–31G* basis set. The first step of the calculations was the geometry optimization. This step gave the optimized molecular geometry, the population analysis, the atomic net charges and the molecular energy. During the second step the program differentiates the molecular energy function twice with respect to the atomic Cartesian coordinates. This step yielded the vibrational force constants in the Cartesian coordinate system, the normal coordinates as linear combination of the atomic vibrational amplitudes, the fundamental frequencies, the infrared intensities, the Raman intensities and depolarization ratios.

The next step of the calculations was the elaboration of the quantum chemical results. The calculated vibrational force constants were transformed into a chemically more interpretable system (**F** matrix). Besides, the quantum chemical units were changed into SI units. The inverse kinetic energy matrix (**G**) was calculated in the same internal coordinate system. The normal coordinate analysis was followed by the calculation of the eigenvalues and the eigenvectors of the **GF** matrix. The **F** matrix was scaled during the fitting process of the calculated fundamental frequencies to the experimental ones. The next step was the computation of the potential energy distribution (PED) matrix.

The fitted calculated fundamentals, the quantum chemically computed intensities and depolarization ratios built the basis for the simulation of the infrared and Raman spectra. Home-made programs were applied to the normal coordinate analysis and the spectrum simulations. Lorentz band contours were applied with 15 cm^{-1} FWHH.

The experimental spectra were analyzed with the PCCAP software [25] for position, intensity, FWHH, shape and overlapping.

4. Results and discussion

One of our previous articles dealt with the vibrational spectroscopy of pinosylvin, 3,5-dihydroxy-*trans*-stilbene [26]. The results on pinosylvin helped us very much in the similar study of resveratrol. Therefore, we compare the two results and, also some results on *trans*-stilbene both from Ref. [33] and from our own work.

4.1. Molecular geometry

At first the conformer with minimal energy was searched. In the first calculation the hydroxyl groups were like in Fig. 1 (conformer ttt). After that the O17-H26 was turned by 180° (conformer ctt), remaining in the ring plane. The next run was the turn of this OH group perpendicular to its ring plane. The consequence of the optimization was its returning into the ring planes. As results of the calculations the ttt conformer was found more stable than the ctt one. Their difference in their molecular energies was 986.2 J mol^{-1}. Therefore, the further calculations were carried out on this conformer, similarly to our calculations on pinosylvin [26]. Furthermore, we regard under the name resveratrol the ttt conformer in this work.

The optimized molecular geometry of resveratrol is presented in Fig. 1, while the numbering of the atoms can be found in Fig. 2, and the optimized geometric parameters are listed in Table 1. Comparing our quantum chemically calculated geometric parameters of the three compounds, namely *trans*-stilbene (TS), pinosylvin (PS) and resveratrol (RV), one can conclude

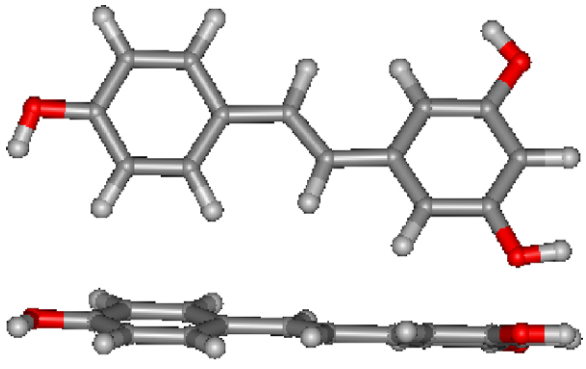

Fig. 1. Optimized molecular structure of ttt-resveratrol, two views.

Table 1
Geometric parameters of *trans*-stilbene (TS), pinosylvin (PS) and resveratrol (RV)

Parameter[a]	X-ray[b]		RHF[c,d]	BLYP[c,e]	B3P86[c]		
	TS[f]	RV[g]	TS		TS[h]	PS[i]	RV[h]
r(C1,C2)	1.403	1.398	1.394	1.420	1.404	1.401	1.399
r(C2,C3)	1.392	1.366	1.384	1.402	1.390	1.395	1.395
r(C3,C4)	1.394	1.391	1.386	1.405	1.392	1.391	1.391
r(C4,C5)	1.396	1.383	1.386	1.409	1.395	1.394	1.397
r(C5,C6)	1.392	1.374	1.384	1.401	1.388	1.393	1.389
r(C1,C6)	1.406	1.399	1.394	1.421	1.405	1.402	1.405
r(C1,C13)	1.471	1.468	1.478	1.470	1.460	1.461	1.461
r(C2,H15)	–	–	1.075	–	1.088	1.088	1.085
r(C3,H/O16)	–	1.379	–	–	1.087	1.360	1.360
r(C4,H17)	–	–	–	–	1.086	1.084	1.087
r(C5,H/O18)	–	1.392	–	–	1.087	1.360	1.361
r(C6,H19)	–	–	1.075	–	1.086	1.087	1.087
r(C7,C8)	1.403	1.396	1.394	1.421	1.405	1.405	1.404
r(C8,C9)	1.392	1.373	1.384	1.401	1.388	1.388	1.386
r(C9,C10)	1.394	1.377	1.386	1.409	1.395	1.395	1.398
r(C10,C11)	1.396	1.371	1.386	1.405	1.392	1.392	1.395
r(C11,C12)	1.392	1.372	1.384	1.402	1.390	1.390	1.386
r(C12,C7)	1.406	1.396	1.394	1.420	1.404	1.404	1.405
r(C7,C14)	1.471	1.460	1.478	1.470	1.460	1.460	1.458
r(C8,H20)	–	–	1.075	–	1.086	1.086	1.086
r(C9,H21)	–	–	–	–	1.087	1.087	1.089
r(C10,H/O22)	–	1.385	–	–	1.086	1.086	1.359
r(C11,H23)	–	–	–	–	1.087	1.087	1.085
r(C12,H24)	–	–	1.075	–	1.088	1.088	1.088
r(C13,C14)	1.341	1.333	1.328	1.362	1.346	1.346	1.347
r(C13,H25)	–	–	1.077	–	1.089	1.089	1.089
r(C14,H26)	–	–	1.077	–	1.089	1.089	1.090
r(O16,H27)	–	–	–	–	–	0.968	0.968
r(O18,H28)	–	–	–	–	–	0.968	0.968
r(O22,H29)	–	–	–	–	–	–	0.968
φ(C1,C2,C3)	121.4	120.3	–	121.5	121.4	120.4	120.3
φ(C2,C3,C4)	120.0	121.5	–	120.1	120.1	120.7	120.7
φ(C3,C4,C5)	119.3	117.9	–	119.4	119.4	118.8	118.9
φ(C4,C5,C6)	120.7	121.8	–	120.6	120.5	121.1	121.0
φ(C5,C6,C1)	120.5	119.8	–	121.0	120.9	120.1	120.0
φ(C6,C1,C2)	118.1	118.7	–	–	117.8	118.8	119.0
φ(C1,C2,H15)	–	–	–	–	118.9	119.6	120.8
φ(C3,C2,H15)	–	–	–	–	119.7	120.0	118.8
φ(C2,C3,H/O16)	–	118.8	–	–	119.7	122.2	117.1
φ(C4,C3,H/O16)	–	119.8	–	–	120.2	117.1	117.1
φ(C3,C4,H17)	–	–	–	–	120.4	120.6	121.9
φ(C5,C4,H17)	–	–	–	–	120.2	120.5	119.2
φ(C4,C5,H/O18)	–	117.8	–	–	120.0	116.7	116.6
φ(C6,C5,H/O18)	–	120.4	–	–	119.5	122.2	122.4
φ(C1,C6,H19)	–	–	–	–	119.9	120.4	120.5
φ(C5,C6,H19)	–	–	–	–	119.1	119.6	119.5
φ(C3,O16,H27)	–	–	–	–	–	108.7	108.8
φ(C5,O18,H28)	–	–	–	–	–	108.7	108.6
φ(C7,C8,C9)	120.5	121.2	–	121.0	120.9	120.9	121.4
φ(C8,C9,C10)	120.5	120.2	–	120.6	120.5	120.5	120.2
φ(C9,C10,C11)	119.3	120.2	–	119.4	119.4	119.4	119.5
φ(C10,C11,C12)	120.0	119.3	–	120.1	120.1	120.1	119.6
φ(C11,C12,C7)	121.4	122.3	–	121.5	121.4	121.3	122.1
φ(C12,C7,C8)	118.1	116.7	–	–	117.8	117.8	117.2
φ(C7,C8,H20)	–	–	–	–	119.9	119.9	120.0
φ(C9,C8,H20)	–	–	–	–	119.1	119.2	118.6
φ(C8,C9,H21)	–	–	–	–	119.5	119.6	119.9
φ(C10,C9,H21)	–	–	–	–	120.0	120.0	119.9
φ(C9,C10,H/O22)	–	119.6	–	–	120.2	120.2	122.7
φ(C11,C10,H/O22)	–	120.2	–	–	120.4	120.3	117.7
φ(C10,C11,H23)	–	–	–	–	120.2	120.2	119.0
φ(C12,C11,H23)	–	–	–	–	119.7	119.8	121.4

Table 1 (*Continued*)

Parameter[a]	X-ray[b]		RHF[c,d]	BLYP[c,e]	B3P86[c]		
	TS[f]	RV[g]	TS		TS[h]	PS[i]	RV[h]
φ(C7,C12,H24)	–	–	–	–	118.9	119.0	118.9
φ(C11,C12,H24)	–	–	–	–	119.7	119.7	119.0
φ(C10,O22,H29)	–	–	–	–	–	–	108.9
φ(C2,C1,C13)	118.8	122.0	119.0	118.6	118.7	118.3	118.2
φ(C6,C1,C13)	123.1	119.3	122.8	–	123.6	122.9	122.8
φ(C7,C14,C13)	126.0	128.5	126.1	127.5	127.0	127.0	127.2
φ(C1,C13,C14)	126.0	126.5	126.1	127.5	127.0	126.7	126.7
φ(C8,C7,C14)	123.1	123.9	122.8	–	123.6	123.5	123.7
φ(C12,C7,C14)	118.8	119.3	119.0	118.6	118.7	118.7	119.1
φ(C1,C13,H25)	–	–	–	–	114.2	114.5	114.3
φ(C14,C13,H25)	–	–	119.0	–	118.7	118.8	118.9
φ(C7,C14,H26)	–	–	–	–	114.2	114.4	114.2
φ(C13,C14,H26)	–	–	119.0	–	118.7	118.6	118.6
φ(Twisting, ring/ring)	6–9	8.0	46.6	–	13.5	18.6	15.0

For the numbering of the atoms see Fig. 2.

[a] Bond lengths (*r*) in angstroms, valence angles (φ) in degrees.

[b] Measured.

[c] Calculated [6–31G(d) basis set].

[d] Ref. [33].

[e] Ref. [34].

[f] Ref. [27].

[g] Ref. [19].

[h] This work.

[i] Ref. [26].

that geometry changed only in the vicinity of the positions of hydroxyl substitutions. A minor change can be found for the twisting angle of the two benzene rings. The double hydroxyl substitution increased this angle, while the third hydroxyl group in the other ring decreased it.

Our TS calculations were compared to the X-ray diffraction results. Hoekstra and Meerten's [27] measured geometric parameters were close in tendencies to our entries. Two very similar structures were found to the TS molecule in crystal. The parameters of the β conformer are listed in Table 1. The parameters of the α conformer differed from those of the β only in some hundred angstroms or some tenth degrees. Two exceptions occurred: in the α conformer the C13–C14 bond length was 1.331 Å and the twisting angle was estimated to 3–4°. Our calculated TS parameters were close to Hoekstra and Meerten's results. The most important source of the differences is the different environments of the molecules, i.e. crystalline and isolated.

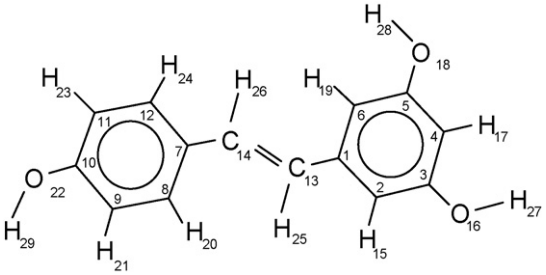

Fig. 2. Numbering of the ttt-resveratrol atoms.

Caruso et al. also [19] studied the crystal structure of RV. Important differences were found between the refined RV skeleton structure and the corresponding TS one. Both the hydroxylic substituents and the strong polar environment with hydrogen bonds distorted the structure. Similarly, differences were also found between Caruso et al.'s results and our calculated RV parameters. These deviations reflect the existence or absence of the intermolecular hydrogen bonds beside the different methods.

4.2. Atomic net charges

The charge distribution on the molecule has important influence on the vibrational spectra. Gaussian 03 offers several methods for the calculation of the atomic net charges. Our previous article on the vibrational spectroscopy of PS [26] contains Mulliken's net charges for TS and PS. For comparison, we calculated these types of net charges also for RV. Beside these calculations we carried out also the natural bond analysis for RV and also for TS and PS.

The comparison of Mulliken's net charges and the atomic natural ones is not an easy task since the theoretical background of the two methods are very different. The definition of Mulliken's charges is based on its population analysis. The *Mulliken population analysis* [28] provides a partitioning of either the total charge density or an orbital density. The number of the electrons in the molecule (*N*) is the integral of the charge density over the space. *N* is partitioned for all atoms considering also the overlap population. According to the theory the overlap population of atoms A and B is divided between the two atoms in half-to-half ratio. This is a weak point of the theory. The other weak point is

its strong dependence on the applied basis set. Our Mulliken's atomic net charges are comparable since the same basis set was applied for all the three molecules. The atomic net charge is the difference between the number of electrons belonging to the atom calculated in this way and the number of electrons of the isolated atom.

The natural atomic charge is based on the theory of the *natural population analysis.* The analysis is carried out with natural bond orbitals (NBO). They are linear combinations of the natural atomic orbitals. The derivation of a valence-shell atomic orbital (NAO) involves diagonalizing of the localized block of the full density matrix of a given molecule associated with basis functions on that atom. A distinguishing feature of NAOs is that they meet the simultaneous requirement of orthonormality and maximum occupancy. In a polyatomic molecule the NAOs mostly retain one-center character, and thus they are optimal for describing the molecular electron density around each atomic center [29]. Natural bond orbitals are linear combinations of the NAOs of the bonded two atoms [30]. The natural population analysis satisfies Pauli's exclusion principle and resolves the basis set dependence problem of the Mulliken's population analysis.

The following conclusions can be driven from the comparison of Mullikan's atomic net charges in TS, PS and RV those are compared in Table 2. All carbon atomic charges of the second (C7–C12) ring changed reacting on the C10 hydroxyl substitution excluding the *para* carbon atom (C7). The charge of C10 changed its sign, while its vicinal carbon atoms became more negative. The conjugation through the vinylidene group (C13–C14) was observed also in the other aromatic ring: C2 became more positive, C4 was more negative in comparison with the corresponding atoms of PS. A similar effect was found also on the H15 and H17 hydrogen atoms: the first became more positive, in contrary, the second one became less positive. The results were quasi-equalizations of the charges of both these oxygen and hydrogen atoms. As it could be expected, the hydroxyl group hydrogens are more positive than the CH ones, the oxygen atoms of the –OH groups have large negative charges.

Certainly, the values of the natural atomic charges are different from Mulliken's atomic net charges (Table 3). The tendencies comparing the PS and RV natural atomic charges are very similar regarding both methods. However, one interesting deviation exists. One can find it in the part of the second ring and the joining part of the vinylidene group. According to Mulliken, C7 and C14 do not change their value practically, while the natural charges of C7 become more negative, that of C14 become more positive as result of the substitution in C10. The atomic net charges of the carbon atoms in the vicinity of C7, C8 and

Table 2
Mulliken's atomic net charges of *trans*-stilbene (ST), pinosylvin (PS) and resveratrol (RV)[a]

Serial number[b]	Atom type	ST[c]	PS[c]	RV[d]
1	C	0.1567	0.1578	0.1568
2	C	−0.2217	−0.3074	−0.2731
3	C	−0.1644	0.3589	0.3598
4	C	−0.1619	−0.2373	−0.2775
5	C	−0.1662	0.3608	0.3608
6	C	−0.2005	−0.2891	−0.2890
7	C	0.1567	0.1565	0.1568
8	C	−0.2005	−0.2002	−0.2079
9	C	−0.1662	−0.1663	−0.2301
10	C	−0.1619	−0.1615	0.3510
11	C	−0.1644	−0.1645	−0.1942
12	C	−0.2217	−0.2210	−0.2304
13	C	−0.2081	−0.2099	−0.2155
14	C	−0.2080	−0.2063	−0.2063
15	H	0.1598	0.1453	0.1673
16	H/O	0.1640	−0.6580	−0.6591
17	H	0.1634	0.1870	0.1628
18	H/O	0.1638	−0.6580	−0.6614
19	H	0.1604	0.1450	0.1430
20	H	0.1604	0.1602	0.1662
21	H	0.1638	0.1645	0.1549
22	H/O	0.1634	0.1644	−0.6515
23	H	0.1640	0.1649	0.1774
24	H	0.1598	0.1592	0.1620
25	H	0.1547	0.1546	0.1542
26	H	0.1547	0.1530	0.1501
27	H		0.4238	0.4243
28	H		0.4238	0.4241
29	H			0.4245

[a] Atomic units.
[b] For the numbering of the atoms see Fig. 2.
[c] Ref. [26].
[d] This work.

Table 3
Natural atomic charges of *trans*-stilbene (ST), pinosylvin (PS) and resveratrol (RV)[a]

Serial number[b]	Atom type	ST	PS	RV
1	C	−0.0759	−0.0434	−0.0420
2	C	−0.2197	−0.3298	−0.3019
3	C	−0.2405	0.3408	0.3415
4	C	−0.2416	−0.3448	−0.3804
5	C	−0.2388	0.3427	0.3445
6	C	−0.2173	−0.3338	−0.3378
7	C	−0.0759	−0.0766	−0.1052
8	C	−0.2173	−0.2176	−0.1966
9	C	−0.2388	−0.2385	−0.3197
10	C	−0.2416	−0.2409	0.3276
11	C	−0.2405	−0.2401	−0.2928
12	C	−0.2197	−0.2194	−0.2014
13	C	−0.2095	−0.2095	−0.2194
14	C	−0.2095	−0.2089	−0.2051
15	H	0.2403	0.2334	0.2518
16	H/O	0.2460	−0.6841	−0.6853
17	H	0.2450	0.2669	0.2484
18	H/O	0.2456	−0.6845	−0.6878
19	H	0.2383	0.2311	0.2302
20	H	0.2383	0.2388	0.2428
21	H	0.2456	0.2460	0.2389
22	H/O	0.2450	0.2455	−0.6822
23	H	0.2460	0.2464	0.2574
24	H	0.2403	0.2402	0.2427
25	H	0.2280	0.2292	0.2294
26	H	0.2280	0.2279	0.2260
27	H		0.4916	0.4920
28	H		0.4915	0.4923
29	H			0.4924

[a] Atomic units.
[b] For the numbering of the atoms see Fig. 2.

Table 4
Internal coordinates and diagonal force constants of *trans*-stilbene (TS), pinosylvin (PS) and resveratrol (RV)

Serial number	Internal coordinate[a]	Scale factors			Diagonal force constants[b]		
		TS	PS	RV	TS	PS	RV
1	$r_{1,2}$	0.910	0.932	0.932	6.318	6.556	6.639
2	$r_{2,3}$	0.910	0.932	0.932	6.686	6.609	6.661
3	$r_{3,4}$	0.910	0.932	0.932	6.654	6.849	6.797
4	$r_{4,5}$	0.910	0.932	0.932	6.536	6.727	6.642
5	$r_{5,6}$	0.910	0.932	0.932	6.763	6.713	6.828
6	$r_{6,1}$	0.910	0.932	0.932	6.187	6.439	6.327
7	$r_{1,13}$	0.993	0.932	0.932	5.514	5.174	5.181
8	$r_{2,15}$	0.904	0.917	0.917	5.069	5.107	5.244
9	$r_{3,16}$	0.904	0.913	0.913	5.113	6.218	6.207
10	$r_{4,17}$	0.904	0.917	0.917	5.127	5.318	5.190
11	$r_{5,18}$	0.904	0.913	0.913	5.111	6.211	6.177
12	$r_{6,19}$	0.904	0.917	0.917	5.127	5.149	5.145
13	$\varphi_{13,6,1} - \varphi_{13,2,1}$	0.993	1.027	1.027	1.016	1.046	1.058
14	$\varphi_{15,1,2} - \varphi_{15,3,2}$	0.936	0.929	0.929	0.522	0.509	0.485
15	$\varphi_{16,2,3} - \varphi_{16,4,3}$	0.936	0.971	0.971	0.505	0.998	0.997
16	$\varphi_{17,3,4} - \varphi_{17,5,4}$	0.936	0.929	0.929	0.503	0.447	0.470
17	$\varphi_{18,4,5} - \varphi_{18,6,5}$	0.936	0.971	0.971	0.509	1.009	1.008
18	$\varphi_{19,5,6} - \varphi_{19,1,6}$	0.936	0.929	0.929	0.519	0.508	0.506
19	$\varphi_{6,2,1} - \varphi_{1,3,2} + \varphi_{2,4,3} - \varphi_{3,5,4} + \varphi_{4,6,5} - \varphi_{5,1,6}$	0.962	0.963	0.963	1.252	1.279	1.279
20	$2\varphi_{6,2,1} - \varphi_{1,3,2} - \varphi_{2,4,3} + 2\varphi_{3,5,4} - \varphi_{4,6,5} - \varphi_{5,1,6}$	0.962	0.963	0.963	1.299	1.272	1.277
21	$\varphi_{1,3,2} - \varphi_{2,4,3} + \varphi_{4,6,5} - \varphi_{5,1,6}$	0.962	0.963	0.963	1.225	1.308	1.304
22	$\theta_{13,6,1,2}$	0.944	0.952	0.952	1.660	1.652	1.659
23	$\theta_{15,1,2,3}$	0.982	0.948	0.948	1.740	1.342	1.476
24	$\theta_{16,2,3,4}$	0.982	0.918	0.918	1.813	1.902	2.238
25	$\theta_{17,3,4,5}$	0.982	0.948	0.948	1.756	1.466	1.312
26	$\theta_{18,4,5,6}$	0.982	0.918	0.913	1.793	2.015	1.999
27	$\theta_{19,5,6,1}$	0.982	0.948	0.948	1.697	1.300	1.289
28	$\tau_{6,1,2,3} - \tau_{1,2,3,4} + \tau_{2,3,4,5} - \tau_{3,4,5,6+}\tau_{4,5,6,1} - \tau_{5,6,1,2}$	0.975	0.952	0.952	0.381	0.328	0.329
29	$\tau_{5,6,1,2} - \tau_{6,1,2,3} + \tau_{2,3,4,5} - \tau_{3,4,5,6}$	0.975	0.952	0.952	0.300	0.318	0.307
30	$\tau_{6,1,2,3} - 2\tau_{1,2,3,4} + \tau_{2,3,4,5} + \tau_{3,4,5,6} - 2\tau_{4,5,6,1} + \tau_{5,6,1,2}$	0.975	0.952	0.952	0.324	0.286	0.298
31	$\upsilon_{25,13}$	0.904	0.917	0.917	5.010	5.089	5.091
32	$\varphi_{25,1,13}$	0.936	0.929	0.929	1.109	1.091	1.094
33	$\tau_{25,13,1,2}$	0.978	0.948	0.948	0.026	0.043	0.039
34	$r_{7,12}$	0.910	0.932	0.932	6.318	6.472	6.423
35	$r_{12,11}$	0.910	0.932	0.932	6.686	6.838	6.980
36	$r_{11,10}$	0.910	0.932	0.932	6.654	6.809	6.696
37	$r_{10,9}$	0.910	0.932	0.932	6.536	6.692	6.546
38	$r_{9,8}$	0.910	0.932	0.932	6.763	6.925	6.961
39	$r_{8,7}$	0.910	0.932	0.932	6.187	6.346	6.386
40	$r_{7,14}$	0.993	0.932	0.932	5.514	5.171	5.221
41	$r_{12,24}$	0.904	0.917	0.917	5.069	5.143	5.152
42	$r_{11,23}$	0.904	0.917	0.917	5.113	5.188	5.250
43	$r_{10,22}$	0.904	0.917	0.917	5.127	5.200	6.244
44	$r_{9,21}$	0.904	0.917	0.917	5.111	5.182	5.101
45	$r_{8,20}$	0.904	0.917	0.917	5.127	5.195	5.205
46	$\varphi_{14,8,7} - \varphi_{14,12,7}$	0.993	1.027	1.027	1.016	1.038	1.018
47	$\varphi_{24,7,12} - \varphi_{24,11,12}$	0.936	0.929	0.929	0.522	0.516	0.516
48	$\varphi_{23,12,11} - \varphi_{23,10,11}$	0.936	0.929	0.929	0.505	0.502	0.476
49	$\varphi_{22,11,10} - \varphi_{22,9,10}$	0.936	0.929	0.971	0.503	0.500	0.971
50	$\varphi_{21,10,9} - \varphi_{21,8,9}$	0.936	0.929	0.929	0.509	0.505	0.502
51	$\varphi_{20,9,8} - \varphi_{20,7,8}$	0.936	0.929	0.929	0.519	0.515	0.513
52	$\varphi_{8,12,7} - \varphi_{7,11,12} + \varphi_{12,10,11} - \varphi_{11,9,10} + \varphi_{10,8,9} - \varphi_{9,7,8}$	0.962	0.963	0.963	1.252	1.252	1.259
53	$2\varphi_{8,12,7} - \varphi_{7,11,12} - \varphi_{12,10,11} + 2\varphi_{11,9,10} - \varphi_{10,8,9} - \varphi_{9,7,8}$	0.962	0.963	0.963	1.299	1.299	1.361
54	$\varphi_{7,11,12} - \varphi_{12,10,11} + \varphi_{10,8,9} - \varphi_{9,7,8}$	0.962	0.963	0.963	1.225	1.227	1.186
55	$\theta_{14,8,7,12}$	0.944	0.952	0.952	1.660	1.666	1.611
56	$\theta_{24,7,12,11}$	0.982	0.948	0.948	1.605	1.554	1.542
57	$\theta_{23,12,11,10}$	0.982	0.948	0.948	1.813	1.749	1.623
58	$\theta_{22,11,10,9}$	0.982	0.948	0.918	1.756	1.705	1.943
59	$\theta_{21,10,9,8}$	0.982	0.948	0.948	1.793	1.738	1.499
60	$\theta_{20,9,8,7}$	0.982	0.948	0.948	1.697	1.644	1.647
61	$\tau_{8,7,12,11} - \tau_{7,12,11,10} + \tau_{12,11,10,9} - \tau_{11,10,9,8} + \tau_{10,9,8,7} - \tau_{9,8,7,12}$	0.975	0.952	0.952	0.381	0.372	0.348
62	$\tau_{9,8,7,12} - \tau_{8,7,12,11} + \tau_{12,11,10,9} - \tau_{11,10,9,8}$	0.975	0.952	0.952	0.300	0.294	0.278

Table 4 (*Continued*)

Serial number	Internal coordinate[a]	Scale factors			Diagonal force constants[b]		
		TS	PS	RV	TS	PS	RV
63	$\tau_{8,24,12,11} - 2\tau_{7,12,11,10} + \tau_{12,11,10,9} + \tau_{11,10,9,8} - 2\tau_{10,9,8,7} + \tau_{9,8,7,12}$	0.975	0.952	0.952	0.322	0.315	0.331
64	$r_{26,14}$	0.904	0.917	0.917	5.010	5.078	5.068
65	$\varphi_{26,7,14}$	0.936	0.929	0.929	1.109	1.092	1.096
66	$\tau_{26,14,7,12}$	0.978	0.948	0.948	0.026	0.040	0.041
67	$r_{13,14}$	0.876	0.932	0.932	8.008	8.525	8.495
68	$\varphi_{13,7,14}$	1.003	1.027	1.027	1.648	1.646	1.648
69	$\varphi_{14,1,13,0}$	1.003	1.027	1.027	1.648	1.660	1.670
70	$\tau_{1,13,14,7}$	1.020	0.952	0.952	0.444	0.418	0.409
71	$\theta_{13,7,14,26}$	0.982	0.948	0.948	1.102	1.130	1.123
72	$\theta_{14,1,13,25}$	0.982	0.948	0.948	1.102	1.134	1.093
73	$r_{27,16}$		0.804	0.804		6.476	6.470
74	$\varphi_{27,3,16}$		0.952	0.952		0.797	0.796
75	$\tau_{27,16,3,4}$		0.985	0.985		0.063	0.063
76	$r_{28,18}$		0.804	0.804		6.474	6.472
77	$\varphi_{28,5,18,}$		0.952	0.952		0.796	0.794
78	$\tau_{28,18,5,4}$		0.985	0.985		0.064	0.064
79	$r_{22,29}$			0.804			6.462
80	$\varphi_{29,10,22}$			0.952			0.791
81	$\tau_{29,22,17,11}$			0.985			0.064

[a] For numbering of the atoms see Fig. 2.
[b] Units: 10^2 N m^{-1} for stretch coordinates and 10^{-18} N m for deformation ones, respectively.

C12 become more negative, while their natural atomic charges show opposite shift.

One can conclude that the natural atomic charges are more sensitive to the changes in the molecular structure than Mulliken's net charges.

4.3. Vibrational force constants

The vibrational force constants of resveratrol together with the definition of the internal coordinates are listed in Table 4. The same data are shown also for the parent molecule *trans*-stilbene and the related molecule pinosylvin. The scale factors for the force constants were transferred from pinosylvin to resveratrol [26]. The calculated vibrational frequencies are in good agreement with the experimental ones (see Table 5). During the discussion of the changes in the force constants we took the pinosylvin set as basis.

The OH substitution at position 10 caused important effects around this position. Of course, the change from H to O in position 22 radically changed the C10–H22 force constant with identical results for the H22–C10 in-plane and out-of-plane bendings. In the environment the force constants of C8–C9 and C9–C10 bonds and also those of out-of-plane bendings of H21–C9 and H23–C11 were the most sensitive to the substitution.

The substitution decreased the twisting angle between the two aromatic rings. This relatively small angle permits the conjugation through the vinylidene group and so the electron effect of OH group in the position 10 can act better on the other ring. The diagonal force constants of the stretchings $r_{1,2}$, $r_{2,3}$ and $r_{5,6}$ increased, while the other three ones decreased. For the CH stretch force constants those of C2–C15 and C4–C17 bonds showed considerable changes. Similarly, force constants of the out-of-plane bendings of the H15–C2, H17–C4 bonds changed in a considerable manner.

4.4. Vibrational frequencies and spectra

Table 5 contains the experimental and calculated vibrational fundamental frequencies and the potential energy distributions for resveratrol. Both resolved measured infrared and Raman frequencies [25] were applied, respectively in the column of the measured spectra. Since experimental spectral data below 150 cm^{-1} were not available, estimated frequencies were used. The value of these frequencies was based on the calculated ones.

The potential energy distributions were calculated from the computed eigenvector matrix L of the GF matrix, according Keresztury and Jalsovszky [31].

It was interesting to investigate the coupling of the OH and CH stretching motions in the corresponding vibrational modes. These are also shown in the table. One can conclude that no coupling exists through the OH groups. Therefore, the CH valence stretching modes are isolated in the ring with double OH substitution. In the other ring, however, the vicinal CH stretchings are coupled, asymmetric and symmetric vibrations exist. In these modes one of the stretchings dominates (that one is listed first). A similar coupling effect was found between the two CH stretch motions of the vinylidene group.

The situation with the coupling of the two OH stretchings is opposite in the same ring, both symmetric and antisymmetric stretchings are determined but they isolate the C4H17 stretching mode.

The other vibrational modes cannot be assigned as group modes. Since the molecule has 81 vibrational modes which we arranged into 18 groups, the participation of these groups

Table 5
Measured and calculated vibrational fundamentals of resveratrol

Measured[a] frequencies (cm^{-1})	Calculated (Becke3P86/6–31G*)				
	Frequencies (cm^{-1})	PED[b](type, %)			
3405	3401	νOH 99	ν[C(3)]OH coupled with ν[C(5)]OH, in-phase		
3397	3400	νOH 99	ν[C(5)]OH coupled with ν[C(3)]OH, anti-phase		
3380	3398	νOH 99	ν[C(10)]OH		
3103	3096	νCHr 99	νC(11)H, coupled with νC(12)H, in-phase		
3103	3091	νCHr 99	νC(6)H		
3082	3081	νCHr 98	νC(8)H, coupled with νC(9)H, in-phase		
3082	3075	νCHr 99	νC(4)H		
3060	3062	νCHr 98	νC(12)H, coupled with νC(11)H, anti-phase		
3060	3060	νCHr 98	νC(2)H		
3056	3047	νCHr 94	νC(9)H, coupled with νC(8)H, anti-phase		
3029	3042	νCHv 93	νC(13)H, coupled with νC(14)H, anti-phase		
3029	3032	νCHv 97	νC(14)H, coupled with νC(13)H, in-phase		
1673	1663	νCCv 60	βCHv 19	νrg 13	
1634	1639	νrg 66	βCHr 10		
1626	1630	νrg 63	βCHr 13		
1613	1617	νrg 59	βCHr 13		
1603	1603	νrg 66			
1514	1520	βCHr 41	νrg 37		
1507	1509	νrg 39	βCHr 30	βOH 11	
1474	1482	νrg 44	βCHr 17	βOH 11	
1444	1445	νrg 46	βCHr 27		
1385	1377	νrg 64	βCHv 11	βOH 11	
1357	1372	νrg 34	νCO 26	βrg 11	νCCv 13
1348	1358	νrg 56	βOH 16	βCHr 11	
1332	1327	βCHv 52	νCCv 19	βCCv 12	βCHr 10
1314	1316	βCHr 47	βCHv 20	βCCv 10	
1304	1301	βCHr 52	βOH 16	νrg 14	
1274	1282	νCO 49	νrg 22	βCHr 18	
1265	1264	βCHv 22	βCHr 19	νCCv 18	νrg 17
1217	1216	βCHv 28	βCHr 20	νrg 16	βOH 15	νCCv 12
1206	1201	βOH 48	βCHr 18	νrg 16	
1177	1187	βOH 31	βCHr 23	νCO 18	νrg 17
1169	1177	βOH 51	νrg 24	βCHr 21	
1162	1163	βCHr 73	νrg 19		
1154	1153	βCHr 47	νCO 23	βOH 18	
1150	1146	βCHr 51	νCCv 18	νrg 14	
1107	1099	βCHr 57	νrg 33		
1014	1014	νrg 44	νCO 19	βCHr 14	
1010	1002	νrg 40	βrg 40	βCHr 17	
997	993	νrg 41	νCO 14	νCCv 13	βCHr 10
988	987	βrg 54	νrg 43		
966	974	γCHv 87			
935	931	γCHr 91			
895	907	γCHr 81			
869	867	γCHv 55	γCHr 22	γCCv 10	
864	865	νrg 52	βCCv 11		
832	823	γCHr 71			
806	805	γCHr 63	γCHv 14		
806	801	βrg 28	νCO 18	βCCv 10	νrg 22
779	789	γCHr 86			
772	784	γCHr 69	γCO 14		
760	768	γCHr 69			
717	707	τrg 64	γCCv 13	γCO 11	
676	678	νrg 22	νCCv 13	νCO 12	βrg 30	βCCv 11
651	667	τrg 78			
643	644	βrg 68	νrg 13		
585	595	γCO 75	τrg 16		
578	592	γCCv 40	γCO 30	τrg 21	
554	558	βCO 37	βCCv 28	βrg 13	
549	541	βrg 46	νCO 13	νrg 14	βCCv 13
519	511	βrg 77			
514	506	γCO 31	τrg 30	γCCv 18	γCHr 13

Table 5 (*Continued*)

Measured[a] frequencies (cm^{-1})	Calculated (Becke3P86/6–31G*)			
	Frequencies (cm^{-1})	PED[b](type, %)		
499	491	βrg 75		
457	443	βCO 42	βCCv 32	βrg 15
410	409	τrg 96		
381	378	βCO 46	βCCv 20	νrg 11
381	374	τOH 88		
376	369	τOH 72		
351	365	τrg 28	τOH 28	γCCv 25
351	360	τOH 94		
324	333	νrg 12	βCO 71	
258	254	τrg 58	γCCv 23	
247	235	τrg 63	βCCv 10	
238	227	τrg 37	βCCv 16	νCCv 15
214	214	τrg 52	γCO 29	
199	173	τrg 40	γCHv 16	γCCv 14
154	163	βCCv 49	τrg 13	
79	78	γCHv 55	βCCv 22	τrg 15
53	53	βCCv 72	γCHv 15	
43	42	γCCv 81	τrg 15	
14	14	γCHv 97		

Mean deviation between measured and calculated frequencies: 6.38 cm^{-1}. Mean relative deviation between measured and calculated frequencies: 1.15%.

[a] Below 150 cm^{-1}: estimated data (see text).

[b] ν: stretch; β: in-plane bend; γ: out-of-plane bend; τ: torsion; r, rg: ring; v: vinylidene.

is very often below 10%. This fact yielded that the sum of the participation percents is sometimes much less than 100%.

As it was mentioned, the scale factors of pinosylvin were applied [26]. Their transfer was very successful since the main absolute deviation between the measured and calculated frequencies was 6.38 cm^{-1}, while the corresponding relative value was 1.15%.

The measured and calculated (simulated) spectra of resveratrol are presented in Fig. 3. The νOH bands overlap with each other, and are broad and intense in the experimental infrared spectrum in contrary to the simulated one of the isolated molecule, where the intermolecular interactions do not act. The experimental Raman spectrum does not contain νOH band. This is very weak also in the simulated one. The ring stretching bands between 1700 and 1600 cm^{-1} are the far most intense ones in both experimental and simulated Raman spectra. These bands dominate. Therefore, we extracted the weaker bands to the inserted spectra. The CH stretch bands are weak in all the four spectra.

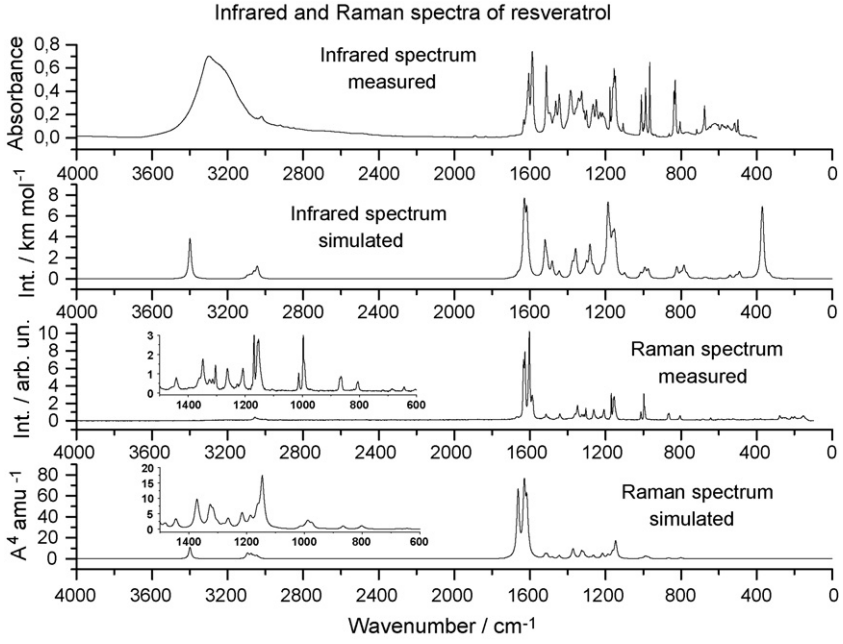

Fig. 3. Infrared and Raman spectra of resveratrol. The experimental Raman spectra were recorded at 1064 nm excitation wavelength.

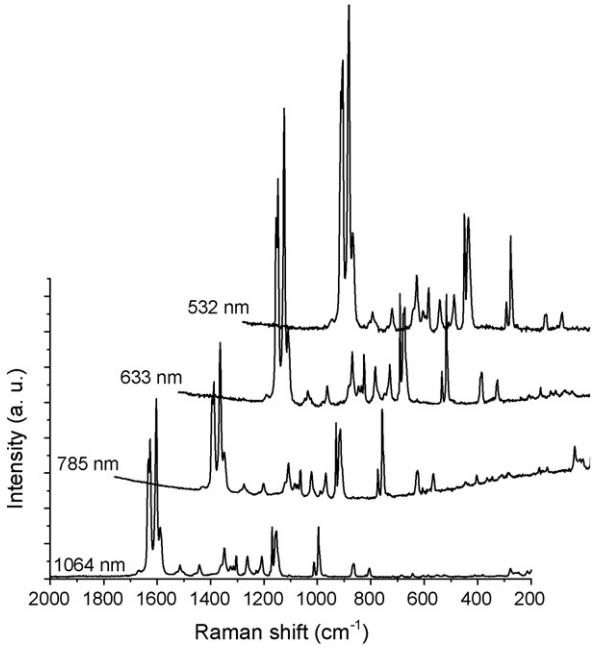

Fig. 4. Raman spectra of resveratrol recorded at different excitation wavelengths (excitation wavelengths are indicated on the graph).

We studied the effect of the excitation wavelength on the Raman spectra of resveratrol for a better determination of the position of the Raman bands. As can be seen in Fig. 4, the locations of the Raman lines do not differ significantly, only the intensity ratio of the different bands alters somewhat.

As known (see e.g. [32]), the Raman intensity of bands are proportional with the fourth power of the absolute frequency, consequently, the ratio of Raman bands at around 1600 and 1000 cm^{-1} (I(1600)/I(1000)) should be higher when the excitation wavelength is 1064 nm than e.g., 532 nm. Our spectra do not follow this trend: while the excitation wavelength is 1064, 785, 633 nm and 532 nm, the ratios I(1600)/I(1000) are approximately 3.2, 1.6, 2.7 and 3.3, respectively. The deviations of the spectra obtained at 1064 nm excitation wavelength were expected since they were recorded on a different instrument and our spectra were not corrected for instrument response function.

5. Conclusions

It was interesting to compare some properties of a series of stilbenoid molecules: *trans*-stilbene, pinosylvin and resveratrol. Obviously, the OH substitutions altered the molecular geometry, the charge distribution, and the vibrational spectra of *trans*-stilbene. It could not be expected that the new OH substitution to pinosylvin decreased the twisting angle between the two rings.

The scale factors of the pinosylvin molecule were transferable to resveratrol without further ado. This is proved by the excellent agreement between the measured and calculated vibrational frequencies of resveratrol.

With respect of the coupling between the group stretchings one can conclude that the OH groups isolate the CH stretchings while the CH groups do not isolate the OH stretchings.

These spectroscopic results could help to understand the basis of the diverse beneficial biological activities of resveratrol and related compounds. The enzymatic methylation and demethylation of these compounds play an important role in the regulation of the formaldehyde concentration in cells.

Acknowledgment

The authors would like to thank Dr. Andrea Szép for the measurement some of the Raman spectra.

References

[1] M. Jang, L. Cai, G.O. Udeani, K.V. Slowing, C.F. Thomas, C.W. Beecher, H.H. Fong, N.R. Farnsworth, A.D. Kinghorn, R.G. Mehta, R.C. Moon, J.M. Pezzuto, Science 275 (1997) 218.
[2] B.B. Aggarwal, A. Bhardwaj, R.S. Aggarwal, N.P. Seeram, S. Sihshodia, Y. Takada, Anticancer Res. 24 (2004) 2783.
[3] P. Langcake, J. Pryce, Physiol. Plant Pathol. 9 (1976) 77.
[4] Y. Takaya, K.-X. Yan, K. Terashima, Y.-H. He, M. Niwa, Tetrahedron 58 (2002) 7259.
[5] Zs. Király-Véghely, E. Tyihák, L. Albert, Zs.I. Németh, Gy. Kátay, Acta Biol. Hung. 49 (1998) 281.
[6] L. Gambelli, G.P. Santaroni, J. Food Comp. Anal. 17 (2004) 613.
[7] L.L. Rudolf, A.V.A. Resurreccion, F.K. Saalia, R.D. Phillips, Food Chem. 89 (2005) 623.
[8] D. Callemien, V. Jerkovic, R. Rozenberg, S.J. Collin, J. Agric. Food Chem. 53 (2004) 424.
[9] C. Counet, D. Callemien, S. Collin, Food Chem. 98 (2006) 649.
[10] S. Renaud, M. de Lorgeril, Lancet 339 (1992) 1523.
[11] K.P.L. Bhat, J.W. Kosmeder, J.M. Pezzuto, Antioxid. Redox. Signal 3 (2001) 1041.
[12] E. Tyihak, Gy. Kátay, Zs. Király-Véghely, Zs.I. Németh, L. Albert, B. Szende, Acta Hortic. 597 (2003) 159.
[13] B. Szende, E. Tyihák, Zs. Király-Véghely, Exp. Mol. Med. 32 (2000) 88.
[14] S.C. Gautam, Y.X. Xu, M. Dumaguin, N. Janakiraman, R.A. Chapman, Bone Marrow Transplant. 25 (2000) 639.
[15] http://www.biologie.uni-freiburg.de/data/bio2/schroeder/CHS_related_superfamily.html#CHS__Mechanisms.
[16] Del Nero F J., C.P. De Melo, Opt. Mater. 21 (2003) 455.
[17] Del Nero F J., C.P. De Melo, Int. J. Quant. Chem. 95 (3) (2003) 213.
[18] H. Cao, X. Pan, C. Li, C. Zhou, F. Deng, T. Li, Bioorg. Med. Chem. Lett. 130 (2003) 1869.
[19] F. Caruso, J. Tanski, A. Villegas-Estrada, M. Rossi, J. Agric. Food Chem. 52 (24) (2004) 7279.
[20] A. Edelmann, J. Diewok, K.C. Schuster, B. Lendl, J. Agric. Food Chem. 49 (2001) 1139.
[21] J.D. Scanlan, D. Bernhardson, J.M. Smith, Proceedings of the 227th ACS National Meeting Anaheim on Resonance Raman and Computational Study of Resveratrol and Related Stilbene Derivatives, CA, 2004.
[22] C.-H. Lin, Y.-H. Chen, Electrophoresis 22 (2001) 2574.
[23] C. Dominguez, D.A. Guillén, C.G. Barroso, J. Chromatogr. A 918 (2001) 303.
[24] M.J. Frisch, G.W. Trucks, H.B. Schlegel, G.E. Scuseria, M.A. Robb, J.R. Cheeseman, J.A. Montgomery Jr., T. Vreven, K.N. Kudin, J.C. Burant, J.M. Millam, S.S. Iyengar, J. Tomasi, V. Barone, B. Mennucci, M. Cossi, G. Scalmani, N. Rega, G.A. Petersson, H. Nakatsuji, M. Hada, M. Ehara, K. Toyota, R. Fukuda, J. Hasegawa, M. Ishida, T. Nakajima, Y. Honda, O. Kitao, H. Nakai, M. Klene, X. Li, J.E. Knox, H.P. Hratchian, J.B. Cross, C. Adamo, J. Jaramillo, R. Gomperts, R.E. Stratmann, O. Yazyev, A.J. Austin, R. Cammi, C. Pomelli, J.W. Ochterski, P.Y. Ayala, K. Morokuma, G.A. Voth, P. Salvador, J.J. Dannenberg, V.G. Zakrzewski, S. Dapprich, A.D. Daniels, M.C. Strain, O. Farkas, D.K. Malick, A.D. Rabuck, K. Raghavachari, J.B. Foresman, J.V. Ortiz, Q. Cui, A.G. Baboul, S. Clifford, J. Cioslowski, B.B. Stefanov, G. Liu, A. Liashenko, P. Piskorz, I. Komaromi, R.L. Martin, D.J.

Fox, T. Keith, M.A. Al-Laham, C.Y. Peng, A. Nanayakkara, M. Challacombe, P.M.W. Gill, B. Johnson, W. Chen, M.W. Wong, C. Gonzalez, J.A. Pople, Gaussian 03, Revision C. 02, Gaussian Inc., Wallingford, CT, 2004.
[25] J. Varga, J. Lejtovicz, PCCAP Software, Chemical Research Center, Hungarian Academy of Sciences, Budapest, 1991.
[26] F. Billes, I. Mohammed-Ziegler, H. Mikosch, A. Holmgren, J. Phys. Chem. A 106 (2002) 6232.
[27] A. Hoekstra, P. Meertens, A. Vos, Acta Crystallogr. B 31 (1975) 2813.
[28] R.S. Mulliken, J. Chem. Phys. 23 (1955) 1833.
[29] A.E. Reed, R.B. Weinstock, F.J. Weinhold, J. Chem. Phys. 83 (1985) 735.
[30] A.E. Reed, F.J. Weinhold, L.A. Curtiss, Chem. Rev. 88 (1988) 899.
[31] G. Keresztury, G. Jalsovszky, J. Mol. Struct. 10 (1971) 304.
[32] G. Keresztury, Raman spectroscopy, in: J.M. Chalmers, P.R. Griffiths (Eds.), Theory in Handbook of Vibrational Spectroscopy, vol. 1, John Wiley & Sons Ltd., Chirchester, 2002, p. 71.
[33] G.N. Andreev, E.H. Korte, B.N. Jordanov, B. Schrader, J. Mol. Struct. 408–409 (1997) 305.
[34] G. Baranović, Z. Meić, A.H. Maulitz, Spectrochim. Acta A 54 (1998) 1017.